Zhuang et al. Nanoscale Research Letters (2016) 11:439
DOI 10.1186/s11671-016-1660-x

Nanoscale Research Letters

NANO EXPRESS Open Access

Biocompatible/Degradable Silk Fibroin:Poly(Vinyl Alcohol)-Blended Dielectric Layer Towards High-Performance Organic Field-Effect Transistor

Xinming Zhuang[1], Wei Huang[1,2], Xin Yang[3], Shijiao Han[1], Lu Li[3*] and Junsheng Yu[1,3*]

Abstract

Biocompatible silk fibroin (SF):poly(vinyl alcohol) (PVA) blends were prepared as the dielectric layers of organic field-effect transistors (OFETs). Compared with those with pure SF dielectric layer, an optimal threshold voltage of ~0 V, high on/off ratio of ~10^4, and enhanced field-effect mobility of 0.22 cm^2/Vs of OFETs were obtained by carefully controlling the weight ratio of SF:PVA blends to 7:5. Through the morphology characterization of dielectrics and organic semiconductors by utilizing atom force microscopy and electrical characterization of the devices, the performance improvement of OFETs with SF:PVA hybrid gate dielectric layers were attributed to the smooth and homogeneous morphology of blend dielectrics. Furthermore, due to lower charge carrier trap density, the OFETs based on SF:PVA-blended dielectric exhibited a higher bias stability than those based on pure SF dielectric.

Keywords: Biocompatible, Silk fibroin, Poly(vinyl alcohol), Organic field-effect transistor, Bias stability

Background

Organic field-effect transistors (OFETs) have shown enormous development in the past few decades due to their potential use in large area sensor arrays, flat panel displays, and radio frequency identification [1–3]. While OFETs with high field-effect mobility (μ), low operating voltage, and good stability are essential for practical use, many researches were conducted to improve these parameters [4, 5]. Especially, as charge carrier conducting channel lies at dielectric/organic semiconductor interface, the dielectric plays an important role in reduce the working voltage of OFETs. An ideal interface should hold minimum charge carrier trap density, and the dielectric would facilitate growth of the upper organic layer in a bottom gate device structure [6]. Many attempts have been applied to modify the interface of gate dielectric and organic semiconductor, such as inserting buffer layer, molecular self-assembly, and UV/ozone (UVO) treatment [7–9]. Currently, several solution-processed dielectric materials, including polymers, inorganic oxides, hybrids composed of inorganic-organic materials, and self-assembled mono- and multilayers, have been exploited for constructing OFETs [10–14]. Meanwhile, another effective way to modify the interface, blending two or more dielectric materials, has been developed to achieve low operating voltage and optimal threshold voltage [15–17].

On the other hand, biological materials, such as silk fibroin (SF), chicken albumen, and gelatin, are emerging as potential solution-processed dielectric materials since they are biodegradable, biocompatible, environmentally friendly, natural abundant, and do not require complicated chemical synthesis [18–20]. Among the various biological materials, SF has been widely used in field of sensors [21], memory devices [22], and component of dynamic devices [23], owing to its unique characteristics of optical transparency, electrical insulation, and flexibility. Moreover, SF is usually a thin film in an aqueous solution process; thus, it offers a biologically derived and biocompatible analog to the synthetic polymer dielectrics

* Correspondence: lli@cqwu.edu.cn; jsyu@uestc.edu.cn
[3]Co-Innovation Center for Micro/Nano Optoelectronic Materials and Devices, Research Institute for New Materials and Technology, Chongqing University of Arts and Sciences, Chongqing 402160, People's Republic of China
[1]State Key Laboratory of Electronic Thin Films and Integrated Devices, School of Optoelectronic Information, University of Electronic Science and Technology of China (UESTC), Chengdu 610054, People's Republic of China
Full list of author information is available at the end of the article

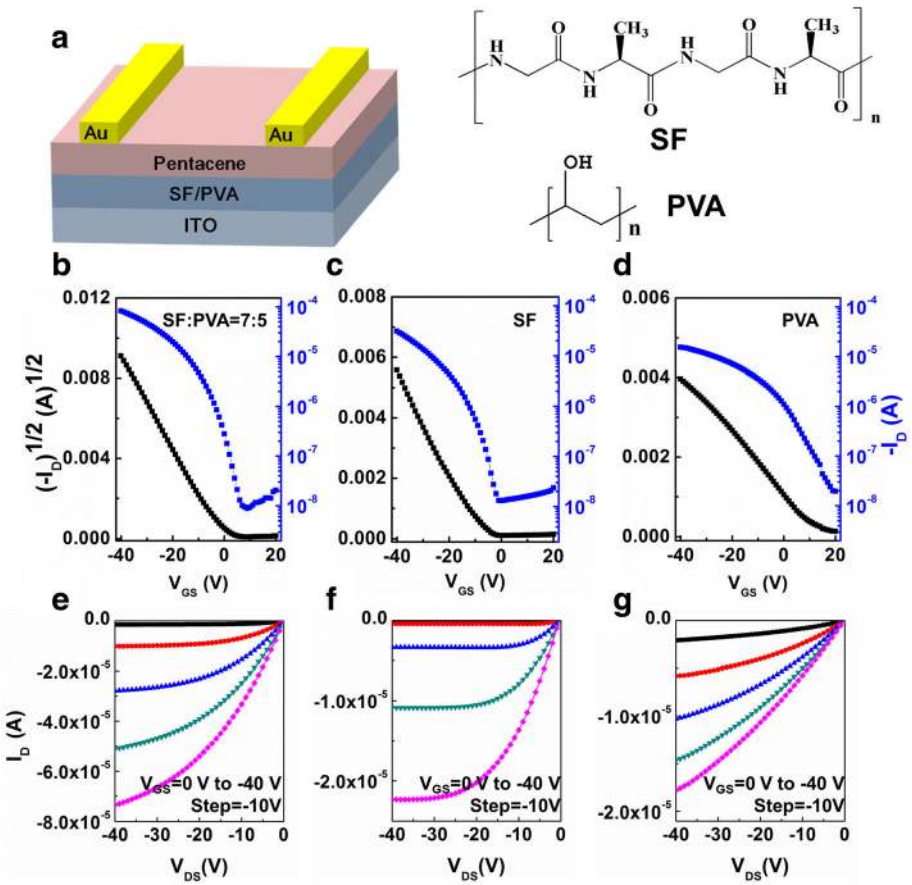

Fig. 1 **a** Schematic structure of OFET based on SF:PVA blends and molecular structures of SF and PVA. **b**–**d** Typical transfer curve (V_{DS} = −40 V) of devices **a**, **b**, and **c**. **e**–**g** Typical output curves (V_{GS} = 0 to −40 V with −10 V step) of devices **a**, **b**, and **c**

traditionally used. Wang et al. reported that silk fibroin as the gate dielectric layer enhanced the crystal qualities of the upper semiconductors and increased the potential of pentacene OFETs as high-speed devices with the ability to compete with a-IGZO TFTs in display technologies [24]. And Tsai et al. reported that silk fibroin can significantly enhance the mobility of n-type C60/pentacene OFET to 1 cm^2/Vs in vacuum [25]. Meanwhile, with a high dielectric constant, dielectric based on SF can reduce the operating voltages [26]. However, SF OFETs are generally limited by bad stability in ambient atmosphere [20]. Poly(vinyl alcohol) (PVA), as a typical polymer dielectric material, has excellent solubility in aqueous solution and high capacitance [27, 28]. Moreover, as the presence of hydroxyl groups (–OH) in PVA, which favored interacting to the carbonyl (–C=O) in SF, the trap density of dielectric layer can be reduced [29]. Hence, the performance and stability of SF-based OFET devices can be dramatically improved by modulating the blends of SF and PVA.

In this work, SF:PVA blends were used to fabricate OFETs as dielectric layers. Through analyzing the electrical characteristics of the devices and the surface morphologies of dielectric and pentacene layers, the surface of SF:PVA blends were more smooth and homogeneous, which leads to an enhanced mobility and optimal threshold voltage. Furthermore, the OFETs based on SF:PVA-blended dielectrics showed a higher bias stability than that based on pure SF under ambient atmosphere due to better dielectric/semiconductor interface property.

Methods

The architecture of the OFETs and chemical structures of SF and PVA are shown in Fig. 1a. An SF aqueous solution with a concentration of ca. 7 wt.% was extracted from cocoons of Chinese silkworm by following the extraction procedure with slight modifications [30]. A 10-g silk was processed 60 min in 0.5 wt.% Na_2CO_3 solution at 100 °C to remove sericin and then rinsed with

Table 1 Capacitance data of SF, SF:PVA = 7:1, SF:PVA = 21:5, SF:PVA = 7:5, SF:PVA = 7:10, and PVA

Dielectric (SF:PVA)	1:0	7:1	21:5	7:5	7:10	0:1
Capacitance data (nF/cm^2)	5.34	5.32	5.23	5.09	5.01	4.51

Table 2 Field-effect mobility (μ), current on/off ratio (I_{on}/I_{off}), threshold voltage (V_T), and sub-threshold (SS) slope of devices A, B, and C

Device	μ (cm^2/Vs)	I_{on}/I_{off}	V_T (V)	SS (V/dec)
A	0.22	9.4×10^3	−1	3.5
B	0.14	2.4×10^3	−11	5.5
C	0.10	0.8×10^3	20	11.0

deionized water and dried at room temperature. The purified fibroin was dissolved in 150 ml of the ternary solvent, $CaCl_2$-ethanol-water (mole ratio = 1:2:8), by stirring at 75 ± 2 °C for 1 h. The solution was centrifuged by centrifugal machine and dialyzed against deionized water for 5 days. At last, the solution was concentrated to ca. 7 wt.% by slow evaporation of deionized water at 60 °C. PVA (Sigma-Aldrich, St. Louis, MO, USA) was dissolved in deionized water with a concentration of 5 wt.%. Then the obtained solutions were mixed at different weight ratios. Indium tin oxide (ITO) glass substrate was cleaned in acetone, deionized water, and isopropyl alcohol for 15 min each by an ultrasonic bath sequentially. The ca. 500 nm SF, PVA, or SF:PVA-blended dielectric was formed by spin-coating at 1600 rpm for 1 min on the substrate at room temperature. Then, the dielectric layer was baked at 70 °C for 1 h to completely remove residual solvents. Consequently, 30 nm pentacene (TCI, Tokyo, Japan) was evaporated under 3×10^{-4} Pa at a rate of 0.2~0.3 Å/s. At last, 50 nm gold source and drain electrodes were thermally evaporated using a metal shadow mask without breaking the vacuum. The length and width of the channel were 100 μm and 1 cm, respectively.

Morphology of SF, SF:PVA-blended dielectrics, and pentacene films were characterized by atom force microscopy (AFM) (MFP-3D-BIO, Asylum Research, Santa Barbara, CA, USA) in tapping mode. Capacitance of the gate dielectrics were obtained by measuring capacitance-frequency properties of ITO/SF/Au, ITO/PVA/Au and ITO/SF:PVA-blended/Au with Agilent 4294A (Santa Clara, CA, USA). Electrical characteristics of the OFETs were measured using a Keithley 4200 (Keithley, Cleveland, OH, USA) in low humidity atmosphere (RH = ~20 %).

Results and Discussion

The capacitance-frequency properties of different dielectric structures (including ITO/SF:PVA-blended/Au, ITO/SF/Au, and ITO/PVA/Au) were tested as shown in Table 1, and leakage currents of these structures were also tested and kept at a relatively low level of 10^{-11}~10^{-9} A in all the dielectrics, as shown in support information Additional file 1: Figure S1.

Devices with different dielectrics were named as device A with SF:PVA = 7:5 blends, device B with pure SF, and device C with only PVA. The transfer and output characteristics of samples A, B, and C are presented in Fig. 1. In the transfer curves, saturation current ($V_{GS} = V_{DS} = -40$ V) of samples B and C are 37.8 and 15.4 μA, respectively,

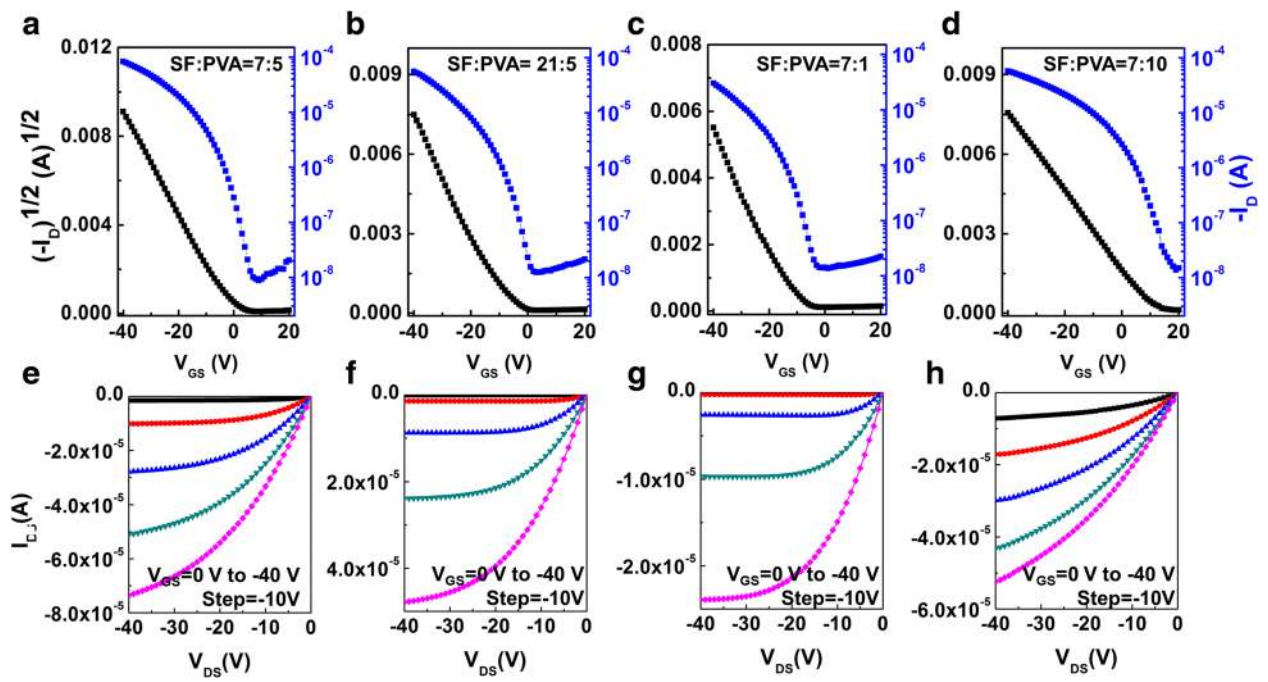

Fig. 2 **a**–**d** Typical transfer curve ($V_{DS} = -40$ V) of devices **d**, **e**, **f**, and **g**. **e**–**h** Typical output curves ($V_{GS} = 0$ to −40 V with −10 V step) of devices **d**, **e**, **f**, and **g**

Table 3 Field-effect mobility (μ), current on/off ratio (I_{on}/I_{off}), threshold voltage (V_T), and sub-threshold slope (SS) of devices D, E, F and G

Device	μ (cm^2/Vs)	I_{on}/I_{off}	V_T (V)	SS (V/dec)
D	0.22	9.4×10^3	−1	3.5
E	0.19	4.5×10^3	−8	4.5
F	0.17	2.1×10^3	−13	5.0
G	0.10	2.9×10^3	10	6.5

while the saturation current of sample A achieves 83.1 μA, which is two times higher than that of the sample B. Meanwhile, device A has a threshold voltage (V_T) of −1 V, which is almost optimal. On the other hand, V_Ts of devices B and C are −11 and ~20 V, which are far from the optimal value of 0 V. It is well known that threshold voltage of OFET is strongly determined by the trap density (N) at the interface of dielectric and organic semiconductor of the device [31]. Low charge trap density at the dielectric/organic semiconductor interface usually benefits to low V_T value. Meanwhile, the trap density (N) at the interface of dielectric and organic semiconductor is proportional to sub-threshold slope (SS) and can be extracted by the Eq. (1):

$$SS = (kT/q)\ln 10(1 + qN/C) \quad (1)$$

where q is the electronic charge, k is Boltzmann's constant, T is absolute temperature, and C is the areal capacitance of the dielectric structure. Through calculation, device A holds a small N of about 1.88×10^{12} cm^{-2} eV^{-1}, while devices B and C show relative large trap densities of 3.12×10^{12} and 5.31×10^{12} cm^{-2} eV^{-1}, respectively. This result reveals that very few ionic impurities reside on the surface of the SF:PVA-blended thin film and thus contributes low charge trap density. As a consequence, a low threshold voltage (−1 V) can be obtained when utilizing SF:PVA blended films.

The saturate field-effect mobility (μ) is obtained from the transfer characteristics in Fig. 1 using Eq. (2):

$$I_D = (W/2L)\mu C(V_{GS} - V_T)^2 \quad (2)$$

where I_D, C, V_{GS}, V_T, W, and L are drain current in the saturation regime, gate capacitance, gate voltage, threshold gate voltage, channel width, and channel length, respectively. The μ of OFETs based on SF:PVA-blended dielectric is about 0.22 cm^2/Vs, higher than that of device with pure SF (0.14 cm^2/Vs) and device with pure PVA (0.10 cm^2/Vs). It is obvious that low trap density in

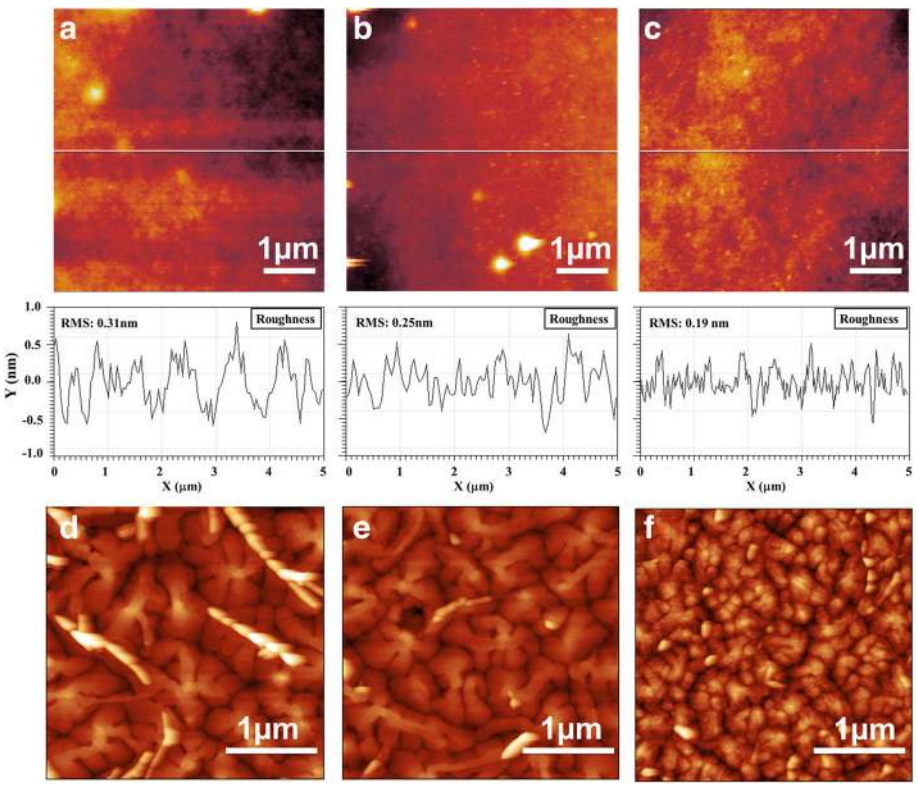

Fig. 3 AFM topography images along with the cross sections of pure SF (**a**), SF:PVA = 21:5 (**b**), and SF:PVA = 7:5 (**c**), respectively (5 μm × 5 μm). AFM images of the pentacene films grown on pure SF (**d**), SF:PVA = 21:5 (**e**), and pure PVA (**f**) dielectric layer (3 μm × 3 μm)

the SF:PVA-blended layer leads to enhancements of both the charge carrier mobility and current on/off ratio. The field-effect mobility (μ), current on/off ratio (I_{on}/I_{off}), V_T, and SS of different devices are summarized in Table 2. As surface roughness is one of the most important properties of dielectric layer, for smooth surface facilitates the formation of good channel layer with less trap states. Thus, surfaces of SF dielectric with/without PVA blends were analyzed through AFM, as shown in Fig. 3. Smooth surfaces were obtained in all the devices, with a root mean square roughness of 0.19 nm on SF:PVA = 7:5 blend layer, and 0.31 nm on pure SF layer. It is well known that the presence of hydroxyl groups (–OH) in PVA will favor interacting to the carbonyl (–C=O) in SF, leading to a smooth and homogeneous morphology [29, 32], thus leading to a high μ value in device based on SF:PVA hybrid gate dielectric. Moreover, according to the higher saturation current in SF:PVA-blended OFETs, and through calculation, OFETs based on SF:PVA-blended dielectric hold a smaller trap density; thus, hydroxyl groups interact with the carbonyl (–C=O) in SF should also introduce low charge trap density at the interface of dielectric and organic semiconductor.

To further optimize the performance of OFETs with SF:PVA blends, a series of OFETs were fabricated by tuning the SF:PVA blends weight ratio to 7:5 (device D), 21:5 (device E), 7:1 (device F), and 7:10 (device G), respectively. Figure 2 depicts the representative transfer plots and output plots of the OFETs with SF:PVA-blended dielectric layers prepared from different weight ratios. It is obvious that a device based on SF:PVA = 7:5 exhibits the best performance with V_T of −1 V, μ of 0.22 cm^2/Vs, and I_{on}/I_{off} of ~10^4, which is the best performance among all of the devices. The electrical parameters of devices with different SF:PVA blend ratios are shown in Table 3. Through calculation, a dielectric with SF:PVA = 7:5 blends has hydroxyl groups (–OH) in PVA one to one interacts to the carbonyl (–C=O) in SF, which contributes to the best smoothness and homogeneous morphology. Furthermore, when the concentration of PVA increases in the dielectric layer, the OFET exhibited inferior performance with high sub-threshold slope, which indicates there are more trap state at interface (N is 3.47×10^{12} cm^{-2} eV^{-1} for SF:PVA = 7:10 blend OFET) [33] (Fig. 3).

In practical use for the display backplane, a continuous bias is usually applied to OFET devices, so the bias

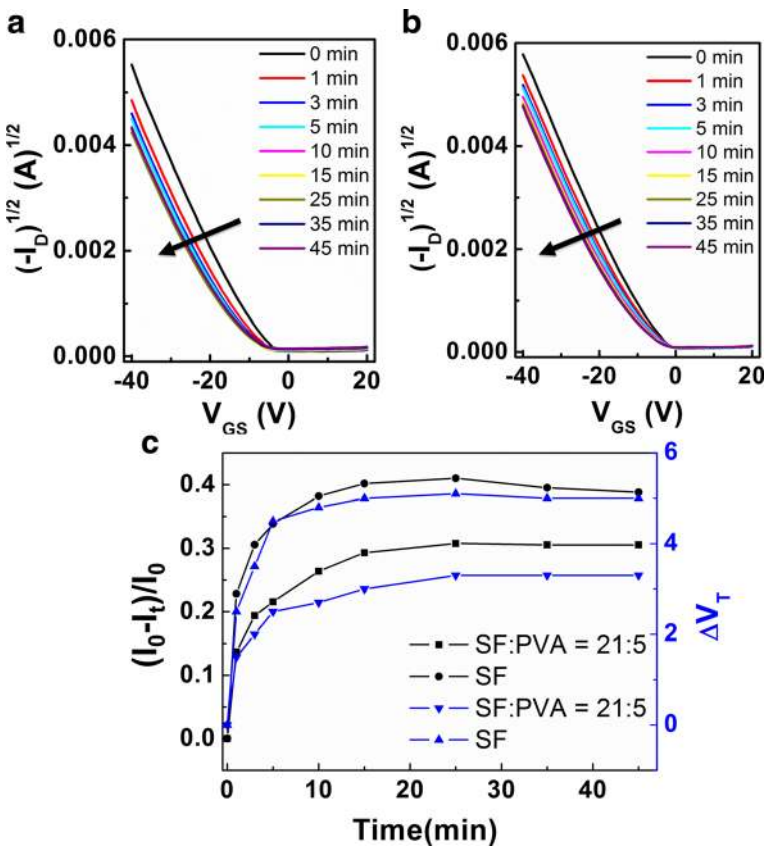

Fig. 4 Threshold voltage shifts (ΔV_T) of OFETs based pure SF (**a**) and SF:PVA = 21:5 blends (**b**), respectively. The bias conditions during the stress were fixed at $V_{GS} = -30$ V, and the transfer curves were measured at the given time intervals. **c** Normalized changes in the currents in OFETs under the bias stress of $V_{GS} = -30$ V

stability is one of the most important parameters of OFETs [34]. Therefore, the bias stabilities of OFETs based on SF:PVA-blended dielectrics were investigated in the atmosphere. Figure 4a, b show negative bias stabilities of OFETs with pure SF and SF:PVA = 21:5 blend dielectrics with a bias stress of $V_{GS} = -30$ V. All the devices show shifts towards the negative gate voltage direction. After 45 min stress, the threshold voltage shift (ΔV_T) of SF:PVA = 21:5 OFETs is about 3 V, which is smaller than that of the pure SF devices ($\Delta V_T = 5$ V). In consistent with the threshold voltage shift, on-current change over time (I_t) reveals similar trend as shown in Fig. 4c, while the field-effect mobility keeps unchanged. It is obvious that OFET with SF:PVA = 21:5 blend dielectric layer shows smaller threshold voltage shift and on-current shift than OFET with pure SF dielectric layer.

As the bias stability is related to the charge trapping effects of the semiconductor/dielectric interface and organic semiconductor film, charge trapping and trap creation under bias stress occur not only within the channel but also throughout the entire semiconductor film [35, 36]. As shown in Fig. 4, by investigating the morphologies of pentacene films grown on different dielectrics through AFM, the crystal of pentacene grown on pure SF is bigger than that on SF:PVA = 21:5 blend dielectric layer, which means fewer grain boundaries exist on pure SF dielectric. Whereas, grain boundary is not the main reason for bias stress related charge trapping [37]. Therefore, the semiconductor/dielectric interface is responsible for the charge trapping events in this work. The surface property of dielectric layer is important to obtain OFETs with a high bias stability [38]. Morphology of SF:PVA = 21:5 blend dielectric is shown in Fig. 3b. Root mean square roughness of 0.25 nm on SF:PVA = 21:5 blend layer is lower than that of pure SF layer (root mean square roughness of 0.31 nm). Therefore, lower charge trap density is obtained in SF:PVA = 21:5 blend device leading to better bias-stress stability of OFETs [39]. However, the OFET with SF:PVA = 7:5 blend dielectric layer exhibits inferior bias stability than the one with pure SF dielectric as shown in support information (Additional file 1: Figure S2). It is probable that a larger amount of hydroxyl groups (–OH) in SF:PVA = 7:5 blends favors interacting to water in ambient atmosphere, which will result in damage of the dielectric layer, leading to a decrease of bias stability [40, 41]. Thus, with less amount of PVA, a better bias-stress stability could be obtained in device E.

Conclusions

In summary, the optimal threshold voltage and enhanced mobility OFETs incorporating with simple biocompatible SF:PVA hybrid dielectric are fabricated, and the property of SF:PVA-blended dielectric was analyzed through AFM. The V_T, μ, and I_{on}/I_{off} of ~0 V, 0.22 cm^2/Vs, and ~10^4, respectively, were obtained in the device with SF:PVA = 7:5 blend dielectrics. Furthermore, the OFET with SF:PVA = 21:5 blend dielectric layer showed a higher bias stability than that with pure SF dielectric. The presence of hydroxyl groups (–OH) in PVA favor interacting with the carbonyl (–C=O) in SF, leading to a smooth and homogeneous morphology, which contributes to lower interface charge trap density. These results indicate that SF:PVA-blended dielectric holds the potential to regulate the performance of OFETs and thus paves a novel way to accelerate the development of nanoscale organic electronic devices.

Additional Files

Additional file 1: Figure S1. (a) Capacitance-frequency characteristics of different dielectric structures (including ITO/SF:PVA-blended/Au, ITO/SF/Au, and ITO/PVA/Au). (b) Leakage current of different dielectric structures. **Figure S2.** (a) Threshold voltage shifts (ΔV_T) of OFETs based SF:PVA = 7:5 blend. The bias conditions during the stress were fixed at $V_{GS} = -30$ V, and the transfer curves were measured at the given time intervals. (b) Normalized changes in the currents in OFETs under the bias stress of $V_{GS} = -30$ V. (DOCX 6196 kb)

Abbreviations

I_{on}/I_{off}: Current on/off ratio; ITO: Indium tin oxide; *N*: Trap density; OFET: Organic field-effect transistor; PVA: Poly(vinyl alcohol); SF: Silk fibroin; SS: Sub-threshold slope; UVO: UV/ozone; V_T: Threshold voltage; μ: Field-effect mobility

Acknowledgements

This research was funded by the National Natural Science Foundation of China (NSFC) (Grant No. 61675041, 51503022), the Foundation for Innovation Research Groups of the National Natural Science Foundation of China (Grant No. 61421002), and Science program of Education Commission of Chongqing (Grant No. KJ1601112). Also, this work was sponsored by Science and Technology Department of Sichuan Province via Grant No. 2016HH0027.

Authors' Contributions

XZ conceived and designed the experiments and wrote the manuscript. XZ, WH, and XY mainly made contribution on the film characterization and analyzed the data. XZ and SH performed the experiments. LL contributed part of the reagents/materials/analysis tools. JY is the supervisor of XZ and the corresponding author of this work. All authors read and approved the final manuscript.

Authors' Information

Xinming Zhuang received his B.A. degree from School of Optoelectronic Information at UESTC in 2014. He has been studying for his Master's degree at State Key Laboratory of Electronic Thin Film and Integrated Devices (SKLETFID) and UESTC since 2014, where his main research interests are in OFETs and OFET-based sensors.

Wei Huang received his B.A. degree from the School of Physics, Nankai University, in 2010. He has been studying for his Ph.D. degree at SKLETFID, UESTC, since 2010, where his main research interests are in OFETs and OFET-based sensors. He has been working as a visiting student at Department of Chemistry and the Materials Research Center Northwestern University since 2014.

Xin Yang got his Ph. D. degree from the Graduate School of Material Science and Technology at Sichuan University in 2013. He is faculty of Chongqing University of Arts and Sciences and deputy director of Co-Innovation Center for Micro/Nano Optoelectronic Materials and Devices majoring in optoelectronic materials and devices.

Shijiao Han received his B.A. degree from the Yingcai Experimental School at UESTC in 2012. He has been studying for his Ph.D. degree at State SKLETFID

and UESTC since 2012, where his main research interests are in OFETs and OFET-based sensors.
Lu Li got his Ph.D. degree from SKLETFID and UESTC in 2012. Now, he is the professor of Chongqing University of Arts and Sciences and deputy director of Co-Innovation Center for Micro/Nano Optoelectronic Materials and Devices majoring in optoelectronic materials and devices.
Junsheng Yu got his Ph.D. degree from Graduate School of Bio-Applications and System Engineering at Tokyo University of Agriculture and Technology in 2001. He is the Professor of SKLETFID and UESTC majoring in organic photoelectronic and electronic materials and devices.

Competing Interests
The authors declare that they have no competing interests.

Author details
[1]State Key Laboratory of Electronic Thin Films and Integrated Devices, School of Optoelectronic Information, University of Electronic Science and Technology of China (UESTC), Chengdu 610054, People's Republic of China. [2]Department of Chemistry and the Materials Research Center Northwestern University, 2145, Sheridan Road, Evanston, IL 60208, USA. [3]Co-Innovation Center for Micro/Nano Optoelectronic Materials and Devices, Research Institute for New Materials and Technology, Chongqing University of Arts and Sciences, Chongqing 402160, People's Republic of China.

Received: 17 July 2016 Accepted: 26 September 2016
Published online: 01 October 2016

References
1. Zhang C, Li J, Han CB, Zhang LM, Chen XY, Wang LD, Dong GF, Wang ZL (2015) Organic tribotronic transistor for contact-electrification-gated light-emitting diode. Adv Funct Mater 25:5625–5632
2. Sablon K (2008) Micrometer- and nanometer-sized organic single crystalline transistors. Nanoscale Res Lett 3:395–396
3. Ford MJ, Wang M, Phan H, Nguyen TQ, Bazan GC (2016) Fullerene additives convert ambipolar transport to p-type transport while improving the operational stability of organic thin film transistors. Adv Funct Mater 26:4472–4480
4. Tavares L, Hansen JK, Hansen KT, Rubahn HG (2011) Organic nanofibers integrated by transfer technique in field-effect transistor devices. Nanoscale Res Lett 6:319
5. Chen H, Dong S, Bai M, Cheng N, Wang H, Li M, Du H, Hu S, Yang Y, Yang T, Zhang F, Gu L, Meng S, Hou S, Guo X (2015) Solution-processable, low-voltage, and high-performance monolayer field-effect transistors with aqueous stability and high sensitivity. Adv Mater 27:2113–2120
6. Khim D, Xu Y, Baeg KJ, Kang M, Park WT, Lee SH, Kim IB, Kim J, Kim DY, Liu C, Noh YY (2016) Large enhancement of carrier transport in solution-processed field-effect transistors by fluorinated dielectric engineering. Adv Mater 28:518–526
7. Khim D, Shin EY, Xu Y, Park WT, Jin SH, Noh YY (2016) Control of threshold voltage for top-gated ambipolar field-effect transistor by gate buffer layer. ACS Appl Mater Inter 8:17416–17420
8. Huang W, Fan H, Zhuang X, Yu J (2014) Effect of UV/ozone treatment on polystyrene dielectric and its application on organic field-effect transistors. Nanoscale Res Lett 9:479
9. Li M, Hinkel F, Mullen K, Pisula W (2016) Self-assembly and charge carrier transport of solution-processed conjugated polymer monolayers on dielectric surfaces with controlled sub-nanometer roughness. Nanoscale 8:9211–9216
10. Sun J, Zhang B, Katz HE (2011) Materials for printable, transparent, and low-voltage transistors. Adv Funct Mater 21:29–45
11. Guo Y, Zhang J, Yu G, Zheng J, Zhang L, Zhao Y, Wen Y, Liu Y (2012) Lowering programmed voltage of organic memory transistors based on polymer gate electrets through heterojunction fabrication. Org Electron 13:1969–1974
12. Zhang P, Li S, Liu C, Wei X, Wu Z, Jiang Y, Chen Z (2014) Near-infrared optical absorption enhanced in black silicon via Ag nanoparticle-induced localized surface plasmon. Nanoscale Res Lett 9:519
13. Li S, Ware M, Wu J, Minor P, Wang Z, Wu Z, Jiang Y, Salamo GJ (2012) Polarization induced pn-junction without dopant in graded AlGaN coherently strained on GaN. Appl Phys Lett 101:122103
14. Jeong SK, Kim MH, Lee SY, Seo H, Choi DK (2014) Dual active layer a-IGZO TFT via homogeneous conductive layer formation by photochemical H-doping. Nanoscale Res Lett 9:619
15. Cho S, Nho SH, Eo M, Lee MH (2014) Effects of processing additive on bipolar field-effect transistors based on blends of poly(3-hexylthiophene) and fullerene bearing long alkyl tails. Org Electron 15:1002–1011
16. Oh JD, Kim DK, Kim JW, Ha YG, Choi JH (2016) Low-voltage pentacene thin-film transistors using Hf-based blend gate dielectrics. J Mater Chem C 4:807–814
17. Li S, Zhang T, Wu J, Yang Y, Wang Z, Wu Z, Chen Z, Jiang Y (2013) Polarization induced hole doping in graded $Al_xGa_{1-x}N$ (x = 0.7 ~ 1) layer grown by molecular beam epitaxy. Appl Phys Lett 102:062108
18. O'Connor TF, Rajan KM, Printz AD, Lipomi DJ (2015) Toward organic electronics with properties inspired by biological tissue. J Mater Chem B 3:4947–4952
19. Zhu B, Wang H, Leow WR, Cai Y, Loh XJ, Han MY, Chen X (2016) Silk fibroin for flexible electronic devices. Adv Mater 28:4250–4265
20. Tsai CL, Tsai LS, Hwang JC (2012) Mobility enhancement by using silk fibroin in $F_{16}CuPc$ organic thin film transistors. Org Electron 13:3315–3318
21. Pal RK, Farghaly AA, Wang C, Collinson MM, Kundu SC, Yadavalli VK (2016) Conducting polymer-silk biocomposites for flexible and biodegradable electrochemical sensors. Biosens Bioelectron 81:294–302
22. Wang H, Zhu B, Wang H, Ma X, Hao Y, Chen X (2016) Ultra-lightweight resistive switching memory devices based on silk fibroin. Small 12:3360–3365
23. Schneider D, Gomopoulos N, Koh CY, Papadopoulos P, Kremer F, Thomas EL, Fytas G (2016) Nonlinear control of high-frequency phonons in spider silk. Nat Mater : , doi:10.1038
24. Wang CH, Hsieh CY, Hwang JC (2011) Flexible organic thin-film transistors with silk fibroin as the gate dielectric. Adv Mater 23:1630–1634
25. Tsai LS, Hwang JC, Lee CY, Lin YT, Tsai CL, Chang TH, Chueh YL, Meng HF (2013) Solution-based silk fibroin dielectric in n-type C60 organic field-effect transistors: mobility enhancement by the pentacene interlayer. Appl Phys Lett 103:233304
26. Shi L, Xu X, Ma M, Li L (2014) High-performance, low-operating voltage, and solution-processable organic field-effect transistor with silk fibroin as the gate dielectric. Appl Phys Lett 104:023302
27. Nam S, Seo J, Kim H, Kim Y (2015) 5 V driving organic non-volatile memory transistors with poly(vinyl alcohol) gate insulator and poly(3-hexylthiophene) channel layers. Appl Phys Lett 107:153302
28. Singh TB, Meghdadi F, Gunes S, Marjanovic N, Horowitz G, Lang P, Bauer S, Sariciftci NS (2005) High-performance ambipolar pentacene organic field-effect transistors on poly(vinyl alcohol) organic gate dielectric. Adv Mater 17:2315–2320
29. Kim GH, Lee D, Shanker A, Shao L, Kwon MS, Gidley D, Kim J, Pipe KP (2015) High thermal conductivity in amorphous polymer blends by engineered interchain interactions. Nat Mater 14:295–300
30. Li M, Lu S, Wu Z, Tan K, Minoura N, Kuga S (2002) Structure and properties of silk fibroin-poly(vinyl alcohol) gel. Int J Biol Macromol 30:89–94
31. Yadav S, Ghosh S (2016) Amorphous strontium titanate film as gate dielectric for higher performance and low voltage operation of transparent and flexible organic field effect transistor. ACS Appl Mater Inter 8:10436–10442
32. Lee KH, Baek DH, Ki CS, Park YH (2007) Preparation and characterization of wet spun silk fibroin/poly(vinyl alcohol) blend filaments. Int J Biol Macromol 41:168–172
33. Huang W, Shi W, Han S, Yu J (2013) Hysteresis mechanism and control in pentacene organic field-effect transistors with polymer dielectric. AIP Adv 3:052122
34. Diallo AK, Fages F, Serein-Spirau F, Lère-porte JP, Videlot-Ackermann C (2011) Effect of molecular structure on bias stress effect in organic thin-film transistors. Appl Surf Sci 257:9386–9389
35. Sharma A, Mathijssen SGJ, Smits ECP, Kemerink M, de Leeuw DM, Bobbert PA (2010) Proton migration mechanism for operational instabilities in organic field-effect transistors. Phys Rev B 82:075322
36. Häusermann R, Batlogg B (2011) Gate bias stress in pentacene field-effect-transistors: charge trapping in the dielectric or semiconductor. Appl Phys Lett 99:083303
37. Kim J, Lee SC, Lee HS, Kim CW, Lee WH (2016) Effects of film microstructure on the bias stability of pentacene field-effect transistors. Org Electron 29:7–12
38. Zhang XH, Tiwari SP, Kim SJ, Kippelen B (2009) Low-voltage pentacene organic field-effect transistors with high-k HfO_2 gate dielectrics and high stability under bias stress. Appl Phys Lett 95:223302

39. Choi HH, Lee WH, Cho K (2012) Bias-stress-induced charge trapping at polymer chain ends of polymer gate-dielectrics in organic transistors. Adv Funct Mater 22:4833–4839
40. She XJ, Liu J, Zhang JY, Gao X, Wang S-D (2013) Operational stability enhancement of low-voltage organic field-effect transistors based on bilayer polymer dielectrics. Appl Phys Lett 103:133303
41. Tardy J, Erouel M (2013) Stability of pentacene transistors under concomitant influence of water vapor and bias stress. Microelectron Reliab 53:274–278